JACS ARTICLES

Published on Web 01/20/2010

Formation and Assembly−Disassembly Processes of ZnO Hexagonal Pyramids Driven by Dipolar and Excluded Volume Interactions

Ming Yang,[†] Kai Sun,[‡] and Nicholas A. Kotov*[,†,‡,§]

Department of Chemical Engineering, Department of Material Sciences and Engineering, and Department of Biomedical Engineering, University of Michigan, Ann Arbor, Michigan 48109

Received August 13, 2009; E-mail: kotov@umich.edu

Abstract: ZnO hexagonal pyramids were obtained in hydrophilic media without any traditional stabilizers (capping agents). The absence of a thick organic shell reducing the anisotropy of nanoparticle (NP) interactions, oxide nature of the materials, and new geometry of the nanocrystals makes possible the observation of new self-organization phenomena. Several new features not present in the previous cases of NP self-organization were identified and discussed. The formation of ZnO pyramids involved recrystallization of larger amorphous NPs followed by the multistage disassembly of intermediate aggregates into individual virtually perfectly shaped nanocrystals. The evolution of NPs begins with crystallization of clustered plates within the original amorphous spherical colloids, and then agglomerated truncated pyramids are formed. These agglomerates further transform into chained pyramids, which eventually separate from each other. The crystallization and disassembly processes can be associated with the decrease of potential and anisotropy of the attractive force field around the crystallites represented in part by dipole moments. The reassembly of the pyramids can still be attained via engaging excluded volume interaction after adding similarly charged polymer. Overall, in this system, we see the first examples of (1) coupled crystallization and disassembly process; (2) induced assembly of nanoscale particles using excluded volume interactions, which were previously used only for aggregation of microscale colloids; and (3) nanoparticle assemblies with variable and experimentally verifiable relative orientation of dipoles including head-to-tail, tail-to-tail pairs, and antiparallel chains. Described assemblies of ZnO pyramids with collective behavior of individual building blocks as well as distinct and experimentally controlled stages of assembly and disassembly present a fundamentally interesting nanoparticle system with rich dynamic behavior.

Introduction

Semiconductor nanoparticles (NPs) have attracted much interest for their novel size- and shape-dependent properties, and self-organization phenomena[1] as well as potential technological applications.[2,3] Organization of NPs and other nanoscale building blocks into premeditated one- (1D), two- (2D), and three-dimensional (3D) systems should be considered as one of the key challenges in today's science and engineering. Self-organized systems can provide an elegant solution for the organization of NPs both in simple and in generic structures such as chains[1h,4b] as well as for complex 3D systems, such as "smart" nanoscale reporters.[4c−e] Superstructures based on nanocrystals can possess unique properties that are not found in individual components and are associated with collective behavior of large arrays of quantum objects.[1h,4a,5] Transition from nanometer to micro- and mesoscale assemblies resulting in hierarchically organized structures would also be quite interesting and technologically relevant.

Gaining a better understanding of processes taking place, forces acting between the particles, and hence methods of control of the organizational behavior would be quite critical along this

[†] Department of Chemical Engineering.
[‡] Department of Material Sciences and Engineering.
[§] Department of Biomedical Engineering.

(1) (a) Lee, S. M.; Cho, S. N.; Cheon, J. *Adv. Mater.* **2003**, *15*, 441–444. (b) Holmes, J. D.; Johnston, K. P.; Doty, R. C.; Korgel, B. A. *Science* **2000**, *287*, 1471–1473. (c) Fang, X. S.; Bando, Y.; Gautam, U. K.; Ye, C.; Golberg, D. *J. Mater. Chem.* **2008**, *18*, 509–522. (d) Polleux, J.; Pinna, N.; Antonietti, M.; Niederberger, M. *Adv. Mater.* **2004**, *16*, 436–439. (e) Tang, Z. Y.; Kotov, N. A. *Adv. Mater.* **2005**, *17*, 951–962. (f) Lieber, C. M. *Solid State Commun.* **1998**, *107*, 607–616. (g) Xia, Y. N.; Yang, P. D.; Sun, Y. G.; Wu, Y. Y.; Mayers, B.; Gates, B.; Yin, Y. D.; Kim, F.; Yan, Y. Q. *Adv. Mater.* **2003**, *15*, 353–389. (h) Tang, Z. Y.; Kotov, N. A.; Giersig, M. *Science* **2002**, *297*, 237–240. (i) Tang, Z. Y.; Wang, Y.; Sun, K.; Kotov, N. A. *Adv. Mater.* **2005**, *17*, 358–363.

(2) (a) Li, L. S.; Hu, J. T.; Yang, W. D.; Alivisatos, A. P. *Nano Lett.* **2001**, *1*, 349–351. (b) Burda, C.; Chen, X. B.; Narayanan, R.; El-Sayed, M. A. *Chem. Rev.* **2005**, *105*, 1025–1102. (c) Alivisatos, A. P. *Science* **1996**, *271*, 933–937. (d) Peng, X. G.; Manna, L.; Yang, W. D.; Wickham, J.; Scher, E.; Kadavanich, A.; Alivisatos, A. P. *Nature* **2000**, *404*, 59–61.

(3) (a) Wang, X. D.; Song, J. H.; Liu, J.; Wang, Z. L. *Science* **2007**, *316*, 102–105. (b) Wang, Z. L.; Song, J. H. *Science* **2006**, *312*, 242–246. (c) Huang, M. H.; Mao, S.; Feick, H.; Yan, H. Q.; Wu, Y. Y.; Kind, H.; Weber, E.; Russo, R.; Yang, P. D. *Science* **2001**, *292*, 1897–1899.

(4) (a) Tang, Z. Y.; Zhang, Z. L.; Wang, Y.; Glotzer, S. C.; Kotov, N. A. *Science* **2006**, *314*, 274–278. (b) Tang, Z. Y.; Ozturk, B.; Wang, Y.; Kotov, N. A. *J. Phys. Chem. B* **2004**, *108*, 6927–6931. (c) Lee, J.; Hernandez, P.; Govorov, A. O.; Kotov, N. A. *Nat. Mater.* **2007**, *6*, 291–295. (d) Lee, J.; Govorov, A. O.; Kotov, N. A. *Angew. Chem., Int. Ed.* **2005**, *44*, 7439–7442. (e) Lu, Y.; Liu, G. L.; Kim, J.; Mejia, Y. X.; Lee, L. P. *Nano Lett.* **2005**, *5*, 119–124. (f) Zhang, Z. L.; Tang, Z. Y.; Kotov, N. A.; Glotzer, S. C. *Nano Lett.* **2007**, *7*, 1670–1675.

10.1021/ja906868h

pathway. In this respect, ZnO nanocolloids are one of the most extensively studied materials due to their distinct optical and electrical properties, simplicity of preparation, diversity of nanoscale chemistry, environmental effects, and biocompatibility.[6] A few interesting observations of orientated attachment of ZnO NPs leading to nanorods[7] and 2D/3D self-assembly of ZnO NPs via surfactant- or ligand-assisted method[8] can be used as examples. Other ZnO-based systems with some degree of organization were observed as well, but they are based on high temperature effects or template action of organic molecules.[9,10] Considering the diversity of chemical processes and modification of ZnO as well as its significance for nanoscale devices,[3] the self-organized systems are expected to reveal novel phenomena for this type of nanocolloids.

Specifically, what attracted us to ZnO is the expected abundance of nanocrystals with strong anisotropy, that is, geometrical and force field inequalities along different directions. One needs to admit that the relationship between anisotropy and self-organization might be intuitively traceable but still is not well understood at all. Finding a nice model system that allows for both theoretical and experimental evaluation of this set of phenomena would be quite useful from fundamental[4] and technological standpoints.[1c,e,f] For ZnO, we see a large variety of highly anisotropic nanocolloids, such as nanowires,[11] nanobelts,[12] or nanotubes.[13] At the same time, another key component of anisotropy, that is, intrinsic electrical field inequalities, is also great. Unlike much-studied CdTe or PbSe crystallizing in cubic lattice, ZnO nanocrystals possess hexagonal packing, which intrinsically increases anisotropy due to the associated intrinsic dipole moment along the primary axis of the crystal lattice. So, unlike many classical cubic and hexagonal semiconductor NPs,[1h,4a,14] both components of anisotropy, shape and intrinsic electrical field, can be strong, which might produce an excellent experimental system as well as some interesting new materials and devices.

We started with the development of an appropriate synthetic method of shape-defined ZnO, such as pyramids. No classical stabilizers were used because (1) they reduce the interaction contrast between different directions, and (2) they eventually represent a problem for potential charge transfer between the NPs assembled in a chain or other 1D-, 2D-, or 3D-superstructures. Pyramids are also quite versatile in terms of potential self-organized structures due to multiple facets and multiple modes of pyramid packing in space. We immediately observed a great difference in particle, formation, assembly, and disassembly for ZnO as compared to cadmium[1h] and lead chalcogenide[14b] systems studied before. Unlike typical nucleation and growth stages,[7,14b] ZnO pyramids are forming as a result of disassembly of the intermediate amorphous NPs, which to the best of our knowledge has never been observed/established before. We see crystallization-coupled evolution from amorphous spherical particles with a diameter of ca. 100 nm, to multicrystallite superstructures with gradually decreasing lateral dimensions from ca. 80 to ca. 20 nm, to short particle chains with the length of ca. 50 nm, and eventually to individual hexagonal pyramids. The disassembly process can be understood as the process opposite of self-assembly, but being governed by the same interparticle interactions. Thus, we calculate the dipole moments of the individual crystallites and observe a clear

(5) (a) Talapin, D. V.; Shevchenko, E. V.; Murray, C. B.; Kornowski, A.; Forster, S.; Weller, H. *J. Am. Chem. Soc.* **2004**, *126*, 12984–12988. (b) Bouhelier, A.; Bachelot, R.; Im, J. S.; Wiederrecht, G. P.; Lerondel, G.; Kostcheev, S.; Royer, P. *J. Phys. Chem. B* **2005**, *109*, 3195–3198. (c) Shevchenko, E. V.; Ringler, M.; Schwemer, A.; Talapin, D. V.; Klar, T. A.; Rogach, A. L.; Feldmann, J.; Alivisatos, A. P. *J. Am. Chem. Soc.* **2008**, *130*, 3274–3275. (d) Li, L. S.; Walda, J.; Manna, L.; Alivisatos, A. P. *Nano Lett.* **2002**, *2*, 557–560. (e) Evlyukhin, A. B.; Bozhevolnyi, S. L. *Laser Phys. Lett.* **2006**, *3*, 396–400. (f) Verma, A.; Srivastava, S.; Rotello, V. M. *Chem. Mater.* **2005**, *17*, 6317–6322. (g) Dennis, C. L.; Jackson, A. J.; Borchers, J. A.; Ivkov, R.; Foreman, A. R.; Lau, J. W.; Goernitz, E.; Gruettner, C. *J. Appl. Phys.* **2008**, *103*, ????. (h) Lee, J.; Govorov, A. O.; Dulka, J.; Kotov, N. A. *Nano Lett.* **2004**, *4*, 2323–2330. (i) Choi, W. S.; Koo, H. Y.; Kim, J. Y.; Huck, W. T. S. *Adv. Mater.* **2008**, *20*, 4504–4508. (j) Puntes, V. F.; Gorostiza, P.; Aruguete, D. M.; Bastus, N. G.; Alivisatos, A. P. *Nat. Mater.* **2004**, *3*, 263–268.

(6) (a) Keem, K.; Jeong, D. Y.; Kim, S.; Lee, M. S.; Yeo, I. S.; Chung, U. I.; Moon, J. T. *Nano Lett.* **2006**, *6*, 1454–1458. (b) Nadarajah, A.; Word, R. C.; Meiss, J.; Konenkamp, R. *Nano Lett.* **2008**, *8*, 534–537. (c) Wang, Z. L. *Annu. Rev. Phys. Chem.* **2004**, *55*, 159–196. (d) Ong, B. S.; Li, C. S.; Li, Y. N.; Wu, Y. L.; Loutfy, R. *J. Am. Chem. Soc.* **2007**, *129*, 2750–2751. (e) Sun, B. Q.; Sirringhaus, H. *J. Am. Chem. Soc.* **2006**, *128*, 16231–16237. (f) Klingshirn, C. *ChemPhysChem* **2007**, *8*, 782–803.

(7) Pacholski, C.; Kornowski, A.; Weller, H. *Angew. Chem., Int. Ed.* **2002**, *41*, 1188–1191.

(8) (a) Yang, M.; Pang, G.; Li, J.; Jiang, L.; Liang, D.; Feng, S. *J. Phys. Chem. C* **2007**, *111*, 17213–17220. (b) Sun, B. Q.; Peterson, R. L.; Sirringhaus, H.; Mori, K. *J. Phys. Chem. C* **2007**, *111*, 18831–18835. (c) Sun, B.; Sirringhaus, H. *Nano Lett.* **2005**, *5*, 2408–2413. (d) Kahn, M. L.; Monge, M.; Snoeck, E.; Maisonnat, A.; Chaudret, B. *Small* **2005**, *1*, 221–224. (e) Yao, K. X.; Sinclair, R.; Zeng, H. C. *J. Phys. Chem. C* **2007**, *111*, 2032–2039. (f) Yin, M.; Gu, Y.; Kuskovsky, I. L.; Andelman, T.; Zhu, Y.; Neumark, G. F.; O'Brien, S. *J. Am. Chem. Soc.* **2004**, *126*, 6206–6207.

(9) (a) Yoshida, T.; Minoura, H. *Adv. Mater.* **2000**, *12*, 1219–1222. (b) Choi, K. S.; Lichtenegger, H. C.; Stucky, G. D.; McFarland, E. W. *J. Am. Chem. Soc.* **2002**, *124*, 12402–12403. (c) Xu, F.; Zhang, P.; Navrotsky, A.; Yuan, Z. Y.; Ren, T. Z.; Halasa, M.; Su, B. L. *Chem. Mater.* **2007**, *19*, 5680–5686. (d) Cong, H. P.; Yu, S. H. *Adv. Funct. Mater.* **2007**, *17*, 1814–1820. (e) Mo, M. S.; Lim, S. H.; Mai, Y. W.; Zheng, R. K.; Ringer, S. P. *Adv. Mater.* **2008**, *20*, 339–342. (f) Peng, Y.; Xu, A. W.; Deng, B.; Antonietti, M.; Colfen, H. *J. Phys. Chem. B* **2006**, *110*, 2988–2993. (g) Bai, P.; Wu, P. P.; Yan, Z. F.; Zhou, J. K.; Zhao, X. S. *J. Phys. Chem. C* **2007**, *111*, 9729–9733. (h) Mo, M.; Yu, J. C.; Zhang, L. Z.; Li, S. K. A. *Adv. Mater.* **2005**, *17*, 756–760.

(10) (a) Liu, F.; Cao, P. J.; Zhang, H. R.; Li, J. Q.; Gao, H. J. *Nanotechnology* **2004**, *15*, 949–952. (b) Wang, Z. L. *J. Mater. Chem.* **2005**, *15*, 1021–1024. (c) Wen, J. G.; Lao, J. Y.; Wang, D. Z.; Kyaw, T. M.; Foo, Y. L.; Ren, Z. F. *Chem. Phys. Lett.* **2003**, *372*, 717–722.

(11) (a) Greene, L. E.; Law, M.; Tan, D. H.; Montano, M.; Goldberger, J.; Somorjai, G.; Yang, P. D. *Nano Lett.* **2005**, *5*, 1231–1236. (b) Vayssieres, L. *Adv. Mater.* **2003**, *15*, 464–466. (c) Liu, B.; Zeng, H. C. *J. Am. Chem. Soc.* **2003**, *125*, 4430–4431. (d) Greene, L. E.; Law, M.; Goldberger, J.; Kim, F.; Johnson, J. C.; Zhang, Y. F.; Saykally, R. J.; Yang, P. D. *Angew. Chem., Int. Ed.* **2003**, *42*, 3031–3034. (e) Yang, M.; Pang, G. S.; Li, J. X.; Jiang, L. F.; Feng, S. H. *Eur. J. Inorg. Chem.* **2006**, 3818–3822.

(12) (a) Gao, P. X.; Ding, Y.; Mai, W. J.; Hughes, W. L.; Lao, C. S.; Wang, Z. L. *Science* **2005**, *309*, 1700–1704. (b) Pan, Z. W.; Dai, Z. R.; Wang, Z. L. *Science* **2001**, *291*, 1947–1949. (c) Kong, X. Y.; Ding, Y.; Yang, R.; Wang, Z. L. *Science* **2004**, *303*, 1348–1351.

(13) (a) Yu, H. D.; Zhang, Z. P.; Han, M. Y.; Hao, X. T.; Zhu, F. R. *J. Am. Chem. Soc.* **2005**, *127*, 2378–2379. (b) Zhang, J.; Sun, L. D.; Liao, C. S.; Yan, C. H. *Chem. Commun.* **2002**, 262–263. (c) Zhang, B. P.; Binh, N. T.; Wakatsuki, K.; Segawa, Y.; Yamada, Y.; Usami, N.; Kawasaki, M.; Koinuma, H. *Appl. Phys. Lett.* **2004**, *84*, 4098–4100. (d) Wu, J. J.; Liu, S. C.; Wu, C. T.; Chen, K. H.; Chen, L. C. *Appl. Phys. Lett.* **2002**, *81*, 1312–1314. (e) Sun, Y.; Fuge, G. M.; Fox, N. A.; Riley, D. J.; Ashfold, M. N. R. *Adv. Mater.* **2005**, *17*, 2477–2481. (f) Hu, J. Q.; Li, Q.; Meng, X. M.; Lee, C. S.; Lee, S. T. *Chem. Mater.* **2003**, *15*, 305–308. (g) Vayssieres, L.; Keis, K.; Hagfeldt, A.; Lindquist, S. E. *Chem. Mater.* **2001**, *13*, 4395–4398.

(14) (a) Pradhan, N.; Xu, H. F.; Peng, X. G. *Nano Lett.* **2006**, *6*, 720–724. (b) Cho, K. S.; Talapin, D. V.; Gaschler, W.; Murray, C. B. *J. Am. Chem. Soc.* **2005**, *127*, 7140–7147. (c) Yong, K. T.; Sahoo, Y.; Zeng, H.; Swihart, M. T.; Minter, J. R.; Prasad, P. N. *Chem. Mater.* **2007**, *19*, 4108–4110. (d) Lu, W. G.; Gao, P. X.; Bin Jian, W.; Wang, Z. L.; Fang, J. Y. *J. Am. Chem. Soc.* **2004**, *126*, 14816–14821. (e) Cozzoli, P. D.; Manna, L.; Curri, M. L.; Kudera, S.; Giannini, C.; Striccoli, M.; Agostiano, A. *Chem. Mater.* **2005**, *17*, 1296–1306. (f) Panda, A. B.; Acharya, S.; Efrima, A. *Adv. Mater.* **2005**, *17*, 2471–2474.

reduction of the field component of the anisotropy with the highest dipole found for the first crystallization products and lowest for free individual pyramids. Orientation of truncated pyramids in the intermediate assemblies, such as chains, clearly follows the head-to-tail orientation of the dipoles. Further growth of the NPs results in the reduction of the dipole moment and separation of chains into individual nearly perfect pyramids. Their reassembly was realized by adding similarly charged polymer. This approach is completely different from those used before based on oriented attachment of ZnO[7] or attractive interaction with oppositely charged templates. Here, we engaged excluded volume interactions, which are commonly used for microscale particles but were not exploited yet for nanoscale assemblies. This resulted in the particle assembly in the head-to-head pattern opposite of that observed for original chains. This indicates that the mutual orientation of dipoles in particle assemblies including chains is a subject of relative strength of many interactions and can be controlled by appropriate assembly conditions.

Experimental Section

Synthesis. In a typical method for the preparation of ZnO NPs leading to hexagonal pyramids, 5.5 g of $Zn(Ac)_2 \cdot H_2O$ and 0.2 g of KOH were added into 50 mL of methanol in a 250 mL round-bottom flask. The mixture was then heated to reflux with magnetic stirring for 48 h before being cooled to room temperature. The as-prepared white precipitates were first separated by centrifuge and then dried in a freeze drier for 2 days.

For the reassembly of ZnO pyramids, 0.0016 g of ZnO pyramids was first dispersed into 50 mL of distilled water to form a transparent solution. After that, 50 μL of 1% poly(diallyldimethylammonium chloride) (PDDA) solution (pH = 7.5) was added into 5 mL of as-prepared ZnO pyramids solution. The solution was kept at room temperature for different times (30 min, 5 h, 12 h) before TEM observation.

Characterization. The products obtained after refluxing for 8, 12, 16, 27, and 48 h were taken out from the mixture for centrifuge and then dispersed into water for transmission electron microscopy (TEM) observation on a JEOL 3011 high-resolution electron microscope, and TEM specimens were prepared by dropping an aqueous solution of products on an ultrathin carbon film on a holey carbon support film, 400 mesh grid supplied by Ted Pella, Inc. The specimens were left to dry at room temperature. For the observation of reassembly of ZnO pyramids by PDDA, the preparation method for TEM specimens was the same as above.

UV−vis spectroscopy was carried out on an 8453 UV−vis ChemStation spectrophotometer produced by Agilent Technologies (former HP8453 by Hewlett-Packard). Photoluminescence (PL) spectra were obtained on a Jobin Yvon Horiba FluoroMax-3 instrument. Dynamic light scattering used for zeta-potentials measurements was performed by Zetasizer Nano ZS from Malvern Instruments (Great Britain). We note in this respect that methanol solutions after refluxing for 1−3 h were still transparent and can be directly used to carry out optical spectroscopic measurements. Methanol solution after refluxing for 6 h turned milky and scattered the light strongly. Nevertheless, it was also directly used for UV−vis and PL spectroscopy and TEM observation, because the milky materials after centrifuge at this point are hard to disperse into water.

Samples obtained after freeze-drying of methanol dispersions were characterized by powder X-ray diffraction (XRD) measurement using Rigaku rotating Anode XRD with Cu Kα generated at 20 kV and 100 mA, and a scanning speed of 10°/min.

Quantum Mechanical Calculations. The software package Spartan (Wave function Inc., Irvine, CA) is used for the quantum mechanical calculation. We use the single point energy mode to compute the dipole moment (DM) using the semiempirical parameter model 3 (PM3) method, which typically gives good estimates of DM for inorganic structures with transition metals. More detailed information about the calculations will be given in the Results and Discussion.

Results and Discussion

ZnO pyramids represent a new member among numerous ZnO-based morphologies of nanocolloids, which typically crystallize in wire or plate form.[15] In the conceptual framework presented in the Introduction, the high anisotropy of ZnO pyramids and other NPs with (tri)angular motif made, for instance, from gold, silver, CdSe, NiS, Co_3O_4, Cr_3O_4, NiO, or γ-Fe_2O_3 etc.,[16] is especially attractive for the realization of unique self-organized systems. Until now, all of the successful preparations of ZnO pyramids (either tetrahedral or hexagonal pyramids) were restricted to the high-temperature (around 300 °C) nonhydrolytic route.[17] In such a system, the organic species such as amine,[17a,g] fatty acid,[17c−f,h] or ionic liquid[17b] serve as capping agents. They are believed to be essential for the stabilization of the high-energy polar crystal planes. However, these stabilizers with relatively high molecular weight also prevent many self-organization phenomena from happening by reducing the apparent anisotropy of particle interactions and evening out inequalities of the force field around NPs. They also diminish the effect of short-range forces between the inorganic cores, which were demonstrated to be essential for the formation of complex structures.[4a,f] So, we decided to come up with a method that produced faceted ZnO hexagonal pyramids in a simple aqueous or mixed-solvent alcohol media without any surfactants. The choice of aqueous media against the organic solutions was made because, similarly to the world of biology, aqueous media is probably the best for the observation of self-organization processes. Under these conditions, the pyramids can be potentially assembled into very interesting structures. Some of them have been theoretically

(15) (a) Yao, K. X.; Zeng, H. C. *J. Phys. Chem. B* **2006**, *110*, 14736–14743. (b) Tian, Z. R. R.; Voigt, J. A.; Liu, J.; McKenzie, B.; McDermott, M. J. *J. Am. Chem. Soc.* **2002**, *124*, 12954–12955. (c) Liu, B.; Zeng, H. C. *J. Am. Chem. Soc.* **2004**, *126*, 16744–16746. (d) Lao, J. Y.; Wen, J. G.; Ren, Z. F. *Nano Lett.* **2002**, *2*, 1287–1291. (e) Gao, P. X.; Wang, Z. L. *Small* **2005**, *1*, 945–949. (f) Yang, M.; Pang, G. S.; Jiang, L. F.; Feng, S. H. *Nanotechnology* **2006**, *17*, 206–212. (g) Yan, H. Q.; He, R. R.; Pham, J.; Yang, P. D. *Adv. Mater.* **2003**, *15*, 402–405. (h) Sounart, T. L.; Liu, J.; Voigt, J. A.; Huo, M.; Spoerke, E. D.; McKenzie, B. *J. Am. Chem. Soc.* **2007**, *129*, 15786–15793. (i) Yao, K. X.; Zeng, H. C. *J. Phys. Chem. C* **2007**, *111*, 13301–13308.

(16) (a) Nair, P. S.; Fritz, K. P.; Scholes, G. D. *Small* **2007**, *3*, 481–487. (b) Lofton, C.; Sigmund, W. *Adv. Funct. Mater.* **2005**, *15*, 1197–1208. (c) Kim, F.; Connor, S.; Song, H.; Kuykendall, T.; Yang, P. D. *Angew. Chem., Int. Ed.* **2004**, *43*, 3673–3677. (d) Jun, Y. W.; Choi, J. S.; Cheon, J. *Angew. Chem., Int. Ed.* **2006**, *45*, 3414–3439. (e) Cheon, J. W.; Kang, N. J.; Lee, S. M.; Lee, J. H.; Yoon, J. H.; Oh, S. J. *J. Am. Chem. Soc.* **2004**, *126*, 1950–1951. (f) Jana, N. R.; Chen, Y. F.; Peng, X. G. *Chem. Mater.* **2004**, *16*, 3931–3935. (g) Ghezelbash, A.; Sigman, M. B.; Korgel, B. A. *Nano Lett.* **2004**, *4*, 537–542.

(17) (a) Wang, D. S.; Xie, T.; Peng, Q.; Zhang, S. Y.; Chen, J.; Li, Y. D. *Chem.-Eur. J.* **2008**, *14*, 2507–2513. (b) Zhou, X.; Xie, Z. X.; Jiang, Z. Y.; Kuang, Q.; Zhang, S. H.; Xu, T.; Huang, R. B.; Zheng, L. S. *Chem. Commun.* **2005**, 5572–5574. (c) Choi, S. H.; Kim, E. G.; Park, J.; An, K.; Lee, N.; Kim, S. C.; Hyeon, T. *J. Phys. Chem. B* **2005**, *109*, 14792–14794. (d) Andelman, T.; Gong, Y. Y.; Polking, M.; Yin, M.; Kuskovsky, I.; Neumark, G.; O'Brien, S. *J. Phys. Chem. B* **2005**, *109*, 14314–14318. (e) Zhong, X. H.; Knoll, W. *Chem. Commun.* **2005**, 1158–1160. (f) Zhong, X. H.; Feng, Y. Y.; Zhang, Y. L.; Lieberwirth, I.; Knoll, W. G. *Small* **2007**, *3*, 1194–1199. (g) Zhang, Z. H.; Lu, M. H.; Xu, H. R.; Chin, W. S. *Chem.-Eur. J.* **2007**, *13*, 632–638. (h) Chen, Y. F.; Kim, M.; Lian, G.; Johnson, M. B.; Peng, X. G. *J. Am. Chem. Soc.* **2005**, *127*, 13331–13337.

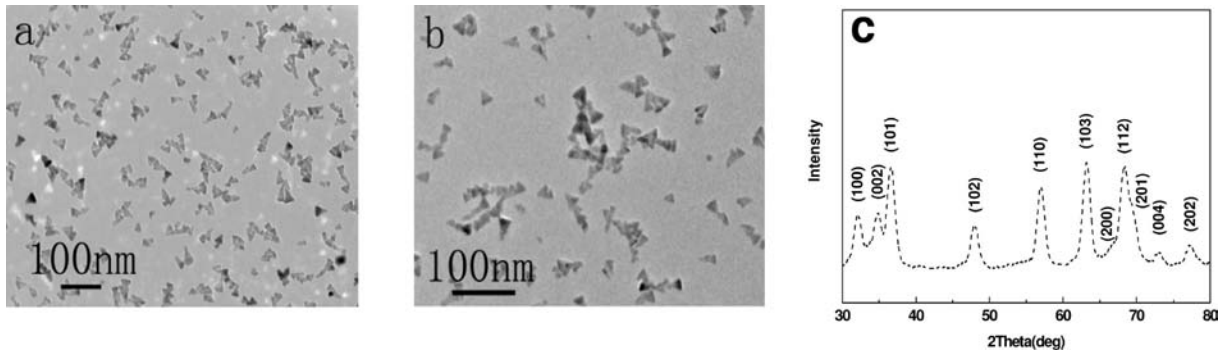

Figure 1. (a,b) TEM images and (c) XRD pattern of ZnO hexagonal pyramids.

simulated but not observed experimentally due to the absence of a suitable experimental system.[18]

Judicious selection of the synthetic conditions and accurate control over pH, precursor concentrations, and refluxing time (t_r) allowed us to find such conditions when electrostatic stabilization of ZnO NPs is strong enough to prevent agglomeration. Moreover, the process of formation of such faceted nanocolloids turned out to involve interesting assembly disassembly phenomena on its own, which expands our understanding of the role of different forces in self-organization.

One of the important requirements to experimental conditions in this case was to control Ostwald ripening and to make it relatively slow even without the surfactant coating, so that the spontaneous particle growth would not dominate in the system. This requires a fine balance of different chemical reactions between different species involved, such as ions, clusters, metal complexes, and NPs. Empirically we were able to find such solution conditions; however, a more quantitative description of these reactions still needs to be established. So, refluxing under conditions specified in the Experimental Section resulted in the formation of ZnO hexagonal pyramids after 48 h, as can be demonstrated by TEM imaging (Figure 1a,b), which was virtually the only product of the synthesis in this case.

Let us first describe the resulting particles, and then the processes leading to their formation. Indeed, the NPs exhibited the attributes of highly anisotropic nanometer scale colloids. The basal and side edge lengths were observed to be of typical length of ca. 15−18 nm. One can clearly see both triangular and hexagonal projections of the nanocrystals (Figure 2). Triangular images correspond to ZnO pyramids lying on the side (Figure 2a), while hexagonal shapes are attributed to the nanocrystals standing up on (probably truncated) apex (Figure 2b). The NPs also seem to attach to each other sometimes (Figure 2c,d), which will be discussed later. All diffraction peaks in XRD pattern (Figure 1c) can be matched to hexagonal phase ZnO (JCPDC card no. 36-1451) and lattice plane spacings from high-resolution electron microscopy images (Figure 2). The XRD peak at 34.4° (Figure 1c) corresponds to the preferred [0001] growth direction of ZnO pyramid. An XRD peak at 31.7° can be matched with lattice spacing of 0.283 nm associated with the distance between two (1000) planes. The observed lattice spacing (Figure 2) of 0.257 nm (Figure 2a,c,d) corresponds to the distance between (0002) crystal planes. The as-prepared ZnO hexagonal pyramids have one (0001) surface for the base and {10-11} planes for side surfaces. XRD pattern and HRTEM data lead to the atomic model presented in Figure 2e and f, which is drawn on the basis of the hexagonal crystal structure of ZnO.

Hexagonal pyramid is not a common shape among many other shapes of ZnO NPs,[11−13] which prompted us to investigate the formation process of ZnO NPs in greater detail to understand the nature of the reactions controlling it as well as to acquire a degree of structural control over ZnO NPs. Against our expectations and many analogous reactions reported,[1,2,7,14,16] the very formation of ZnO pyramids involves not only simple nucleation and growth processes as with II−VI semiconductors,[19] but also transformation and disassembly processes of the original NPs forming much earlier than pyramids.

A series of experiments with different reaction time t_r were carried out. Light scattering of the methanol solution gradually increases by $t_r = 6$ h. Before this, no adsorption characteristics of ZnO can be found in the adsorption spectra (Figure 4a). The observed broad emission peak at ca. 360 nm for $t_r = 1$ and 3 h should be attributed to the amorphous ZnO clusters in the system (Figure 4b). During these initial stages of NP synthesis, the nucleation and cluster ripening stages are taking place, and mostly subnanometer scale particles are present.

Our focus will be primarily on solution events starting at $t_r = 6$ h. At this point of the process, porous quasi-spheres of ca. 100 nm in diameter form (Figure 3a,b) and yield a weak adsorption peak in the UV−vis spectrum (Figure 4a) typically associated with ZnO phase. Because of the amorphous structure, no distinct exciton band can be detected at this point.

When $t_r = 12$ h, the clear shapes of seemingly triangular crystallites in the larger agglomerates of ca. 80 nm in dimensions can be detected. One can conclude that the amorphous spheres recrystallize not into individual NPs but rather into multi NP assemblies (Figure 3c and e). HRTEM images show the parallelism and overlap of lattice fringes, indicating that the triangular shapes of NPs share the same orientation (Figure 3d and f).

For $t_r = 16$ h, elongated triangular agglomerates with lateral size of ca. 60 nm, and chains with an average length of 80 nm are predominantly observed (Figure 3g and h). The ZnO crystallites become bigger, and their shape approaches nearly a fully grown pyramid. They assemble in the chain in the head-to-tail fashion, which can also be traced in the larger aggregates as well.

By $t_r = 48$ h, the elongated triangular agglomerates and chains disassemble into individual pyramids and short chains (Figures

(18) Fejer, S. N.; James, T. R.; Hernandez-Rojas, J.; Wales, D. J. *Phys. Chem. Chem. Phys.* **2009**, *11*, 2098–2104.

(19) Talapin, D. V.; Rogach, A. L.; Haase, M.; Weller, H. *J. Phys. Chem. B* **2001**, *105*, 12278–12285.

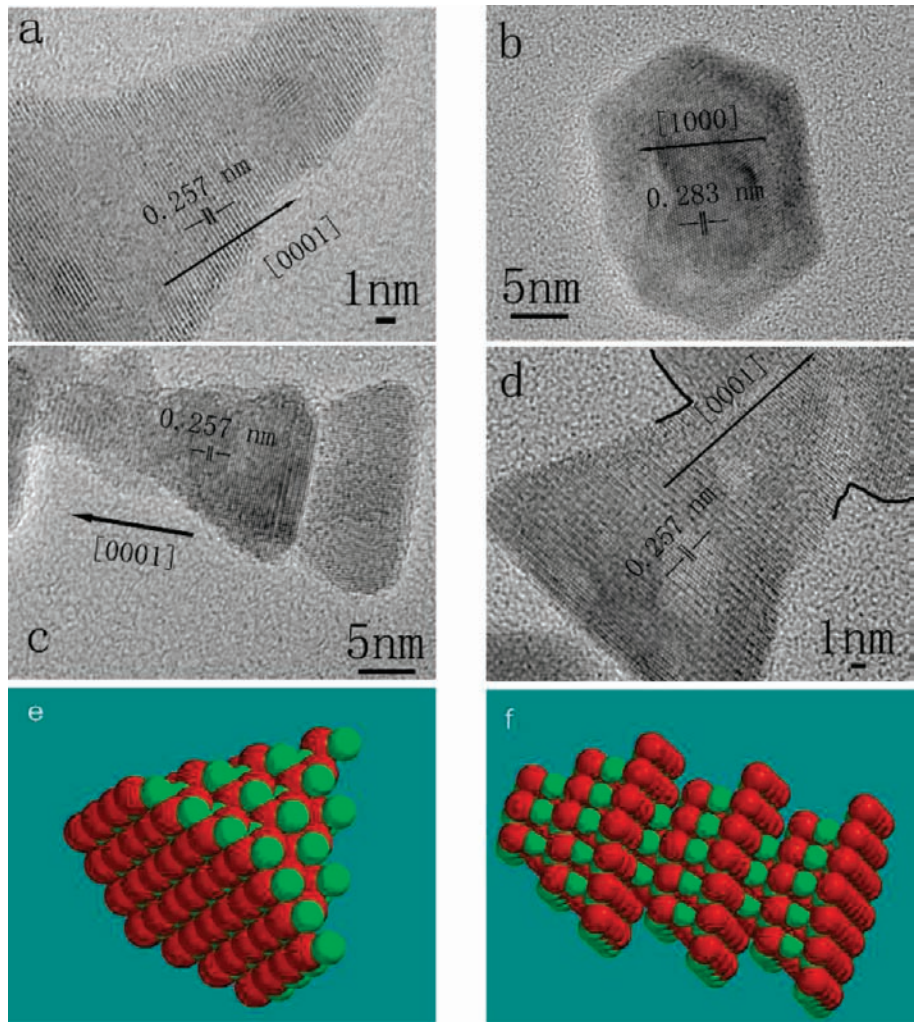

Figure 2. (a−d) HRTEM characterization of ZnO hexagonal pyramids. (e,f) Atomic model of ZnO pyramids observed in (a) and (c), respectively. Zn atoms are green, and O atoms are red.

1 and 3i,j) of an average length of 50 nm. The light scattering measurements (Table 1) indicated that particle size diminished from original 780 to final 48 nm, which was perfectly consistent with TEM observations and confirmed the process of initial assembly in spheres and subsequent disassembly into individual NPs.

The experimental data obtained suggest the formation of ZnO pyramids starts with the growth-coupled nucleation process resulting in porous spheres, followed by recrystallization, and spontaneous partition into freely suspended pyramids. A well-defined exciton band can be observed with enough crystallization time $t_r = 12$ h (Figure 4a). Further increasing t_r does not result in the obvious red-shift of the onsets of adsorption spectra (Figure 4a). As expected, band-edge emission shifts to longer wavelengths with increasing t_r (Figure 4b). However, after 16 h, this shift plateaus, indicating the kinetic stability of the produced ZnO pyramids. A weak broad emission band above 450 nm is also observed. We believe that it results from the recombination of charge carriers on specific defects, such as bulk oxygen vacancies or surface energy traps.[20]

Once sufficient information about the different intermediate stages of the formation of hexagonal pyramids is available, it is possible to consider processes leading to the final products. After the formation of amorphous porous spheres, the growth of ZnO crystals occurs via a continued recrystallization process. The rate of recrystallization is not the same for different parts of spheres. It starts from the outmost surface of the spheres, which is indicative of the likely participation of dissolved Zn^{2+} and OH^- ions from solution, the primary players in Ostwald ripening. The spheres split due to formation of crystal lattice defects at the interface between growing crystal and the remaining sphere. In the high-resolution TEM images, one can see the nascent slits between emerging nanocrystals (Figure 3c,e). Consequently, growing ZnO pyramids partially separate from each other. They are still held together by a multitude of forces whose net sum is attractive. Among these forces, electrostatic repulsion begins to dominate, and this stage is characterized by the formation of multiparticle agglomerates made from crystallites intermediate between amorphous clusters and perfect pyramids (Figure 3g,h). As the crystallization progresses and the balance between attraction and repulsion continued to shift toward separation, these agglomerates split and produce short chains (Figure 3i,j). As the pyramids become more and more perfect, the chains further separate into single pyramids, although linear aggregates are still present. An

(20) Vanheusden, K.; Warren, W. L.; Seager, C. H.; Tallant, D. R.; Voigt, J. A.; Gnade, B. E. *J. Appl. Phys.* **1996**, *79*, 7983–7990.

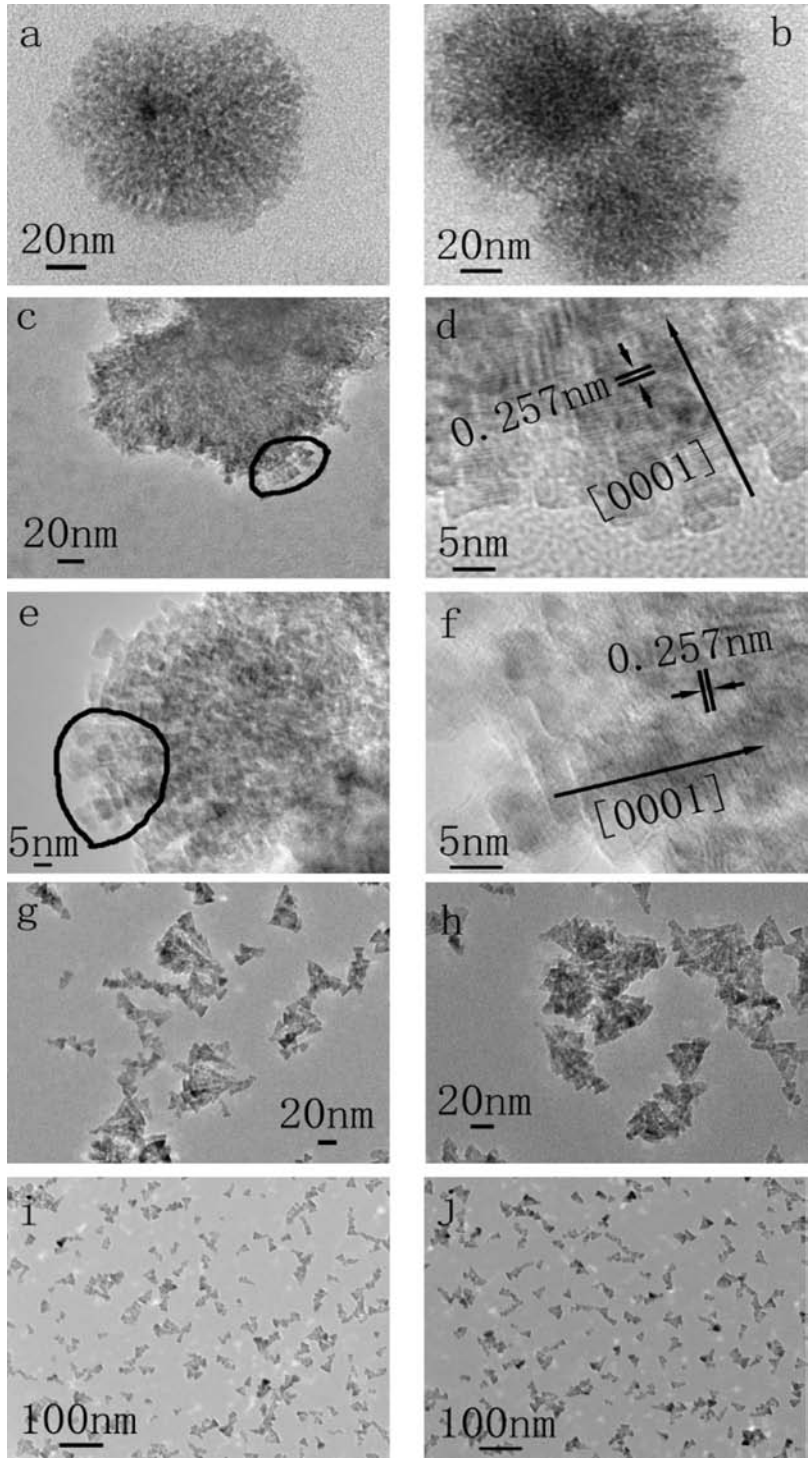

Figure 3. Time-dependent TEM observation of the evolution process for ZnO hexagonal pyramids. (a,b) 6 h. (c−f) 12 h. (g,h) 16 h. (i,j) 48 h. Images d and f are the HRTEM images for the emphasized part by circles in images c and e, respectively.

observation could be made that the better defined crystal surface formed, the greater degree of separation occurred.

To discuss the driving force(s) behind the spontaneously disassembly phenomena, it is important to reiterate that such a process is coupled with the evolution of different degrees of truncation of the pyramids beginning from plates and finally to full pyramids. Therefore, it would be quite useful to have a measure of the force field and anisotropy around individual crystallites. It is also important to mention that assembly and disassembly are the two sides of the same process with just switched direction of the reaction. In our view, the primary structure of the individual particles and their average distance from each other determine whether they assemble or disassemble, but the nature of forces will remain still the same and subject to control by experimental conditions. Understanding what these forces are and what they depend upon is the key in production of assemblies with desirable behavior, properties, and geometry.

The evolution of forces between the particles during this process is quite complex and consists of charge−charge,

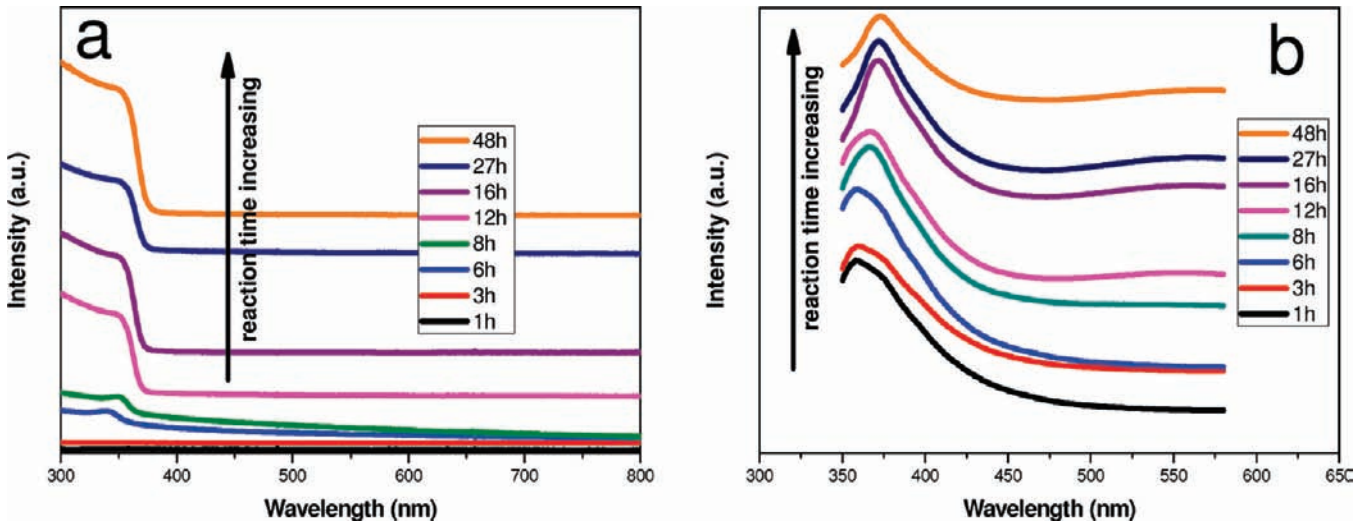

Figure 4. Time-dependent (a) UV−vis spectra and (b) photoluminescence spectra ($\lambda_{excitation}$ = 325 nm, the spectra were shifted with respect to each other along the ordinate for clarity).

Table 1. Dynamic Light Scattering Measurements of Electrokinetic Zeta Potential of Nanocolloids Peak Position of Size Distribution Forming in the Process of the Reaction

reflux time (h)	8	12	16	48
peak position of size distribution (nm)	783.6	62.5	50.3	48.6
zeta potential (mV)	+16.2	+34.9	+36.7	+33.2

charge−dipole, dipole−dipole, induced dipolar, van der Waals, hydrophobic interactions, hydrogen bonding, and probably other smaller components. Many of them are quite difficult to estimate and simulate. Several of them can be discussed in qualitative terms. Two of the components in this palette of forces related to the stationary dipole moment of the particles, *D*, we can evaluate fairly accurately. This will help us to explain in the first approximation the evolution of the particle assembly disassembly patterns. For this purpose, we built atomic models of ZnO nanocrystals taking advantage of the established hexagonal crystal lattice of these particles (Figures 1c and 2). We also assumed that most of the crystal planes are supposed to be O-terminated surfaces because the O-terminated (000-1) polar surface is usually more inert in comparison with the Zn-terminated ZnO (0001) polar surface[21] and are not subject to further oxidation. The exposed oxygen atoms are terminated most of the time with hydrogen atoms due to the aqueous nature of the dispersion. This molecular model correlates well with the structural results from the previous studies of ZnO NPs.[22] The net formal charge on the built model is calculated from the atomic stoichiometry by associating H, Zn, and O with a charge of +1, +2, and −2, respectively. We started from a fairly flat ZnO pyramid (Figure 5a,b) with a cumulative molecular formula of $Zn_{64}O_{19}(OH)_{93}^{3-}$. The pyramids with different degrees of truncation corresponding to the consecutive stages of crystallization can be obtained by adding O and Zn atomic layers to the starting flats (Figure 5a,b). In fact, this process is likely to mimic the actual growth of ZnO pyramids (Figure 5c−h). The bigger truncated pyramids are represented by chemical formulas as $Zn_{83}O_{31}(OH)_{100}^{4+}$, $Zn_{95}O_{38}(OH)_{105}^{9+}$, and $Zn_{105}O_{42}(OH)_{111}^{15+}$. The positive charge associated with the bigger pyramids is consistent with zeta potential results (Table 1). The negative charge of $Zn_{64}O_{19}(OH)_{93}^{3-}$ is quite reasonable as well; it is relevant mostly in the very early stages of transformation of amorphous spheres into small pyramids. It is difficult to evaluate the charge of these flat pyramids experimentally because it is obscured by the charge of the amorphous part of the spherical NPs into which $Zn_{64}O_{19}(OH)_{93}^{3-}$ are integrated (Figure 3a−d).

The geometries of these atomic models were first optimized by using the Merck molecular force field (MMFF) allowing all bonds to acquire a relaxed configuration. We then used single point energy mode to compute dipole moment, *D*, of the equilibrium atomic model using the semiempirical parameter model 3 (PM3) method, which demonstrated reasonable results before.[23] Generally, the directions of *D* in all cases are mainly parallel to the [0001] axis of the pyramids pointed from the tip to the bottom. The slight deviations are associated with distortions of O−H bonds on the surface (Figure 6). On the basis of the calculations (Figure 6 and Table 2), we can clearly see that along with the growth of pyramids, the dipole moment continually decreases from 91.49 *D* for fairly flat $Zn_{64}O_{19}(OH)_{93}^{3-}$ to 25.96 *D* for nearly full pyramid $Zn_{105}O_{42}(OH)_{111}^{15+}$. The change of *D* always happens as a result of the variation of surface electron density. Considering the dependence of the overall dipole moment of NPs on their structure, one also can make a note that the presence of methanol in the media as a cosolvent can result in methoxy substitution of surface OH groups. It is important in this respect to evaluate the effect of such derivatization of ZnO surface because variability of surface groups can potentially cause some assembly processes as well. To clarify this issue, we applied the same quantum mechanical methods to a truncated pyramid displaying the highest *D* but carrying different number of $-O-CH_3$ groups including highly asymmetric distribution with respect to the center of mass. It was found that $-O-CH_3$ groups appear to have negligible contribution to dipole moment in these structures (Figure 7). Therefore, we will consider only simpler −OH terminated NPs in the following parts of this work for now.

(21) Wang, Z. L.; Kong, X. Y.; Zuo, J. M. *Phys. Rev. Lett.* **2003**, *91*, 4.
(22) Kawska, A.; Duchstein, P.; Hochrein, O.; Zahn, D. *Nano Lett.* **2008**, *8*, 2336–2340.
(23) (a) Shanbhag, S.; Kotov, N. A. *J. Phys. Chem. B* **2006**, *110*, 12211–12217. (b) Vinod, T. P.; Yang, M.; Kim, J.; Kotov, N. A. *Langmuir* **2009**, *25*, 13545–13550.

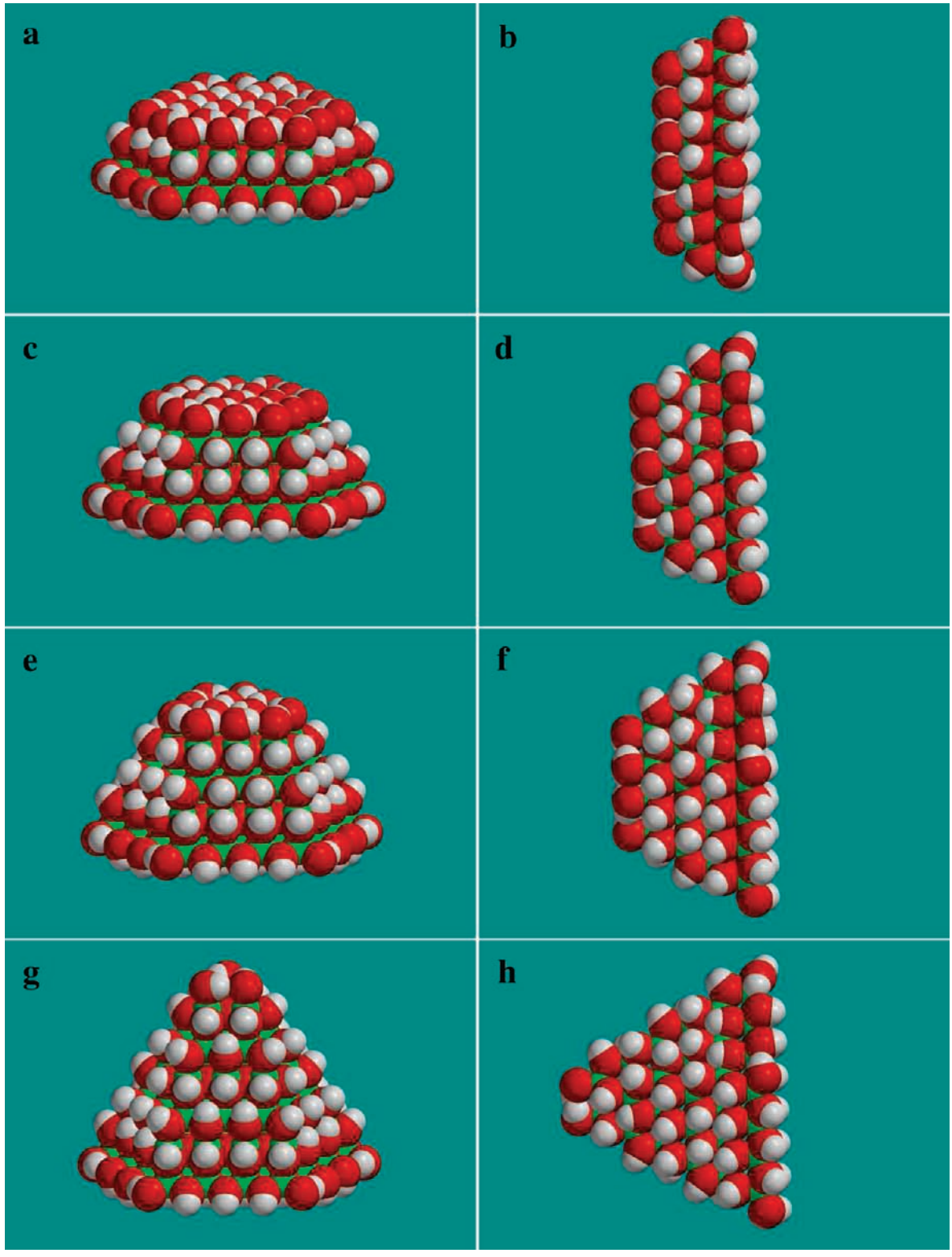

Figure 5. Atomic models in space filling mode from different angles of view of (a,b) $Zn_{64}O_{19}(OH)_{93}^{3-}$, (c,d) $Zn_{83}O_{31}(OH)_{100}^{4+}$, (e,f) $Zn_{95}O_{38}(OH)_{105}^{9+}$, and (g,h) $Zn_{105}O_{42}(OH)_{111}^{15+}$. Zn atoms are green, O atoms are red, and H atoms are white.

The mapping of the value of electrostatic potential onto the electron density surfaces of these pyramidal models may help us to better understand the evolution of *D* (Figure 8). As the pyramids grow (Figure 8a−d), the area of exposed plane on the top becomes smaller, which automatically reduces the negative component of the potential map on the NP (Figure 8a−d). Also, in the same progression, O atoms in the bottom planes become more negative (Figure 8a−d), while the most positive parts of the nanocrystal keep on residing on H atoms of the bottom plane (Figure 8a−c). Note as well that the most positive parts for the largest pyramids calculated, $Zn_{105}O_{42}(OH)_{111}^{15+}$, are located both on H atoms in the bottom and on H atoms at the surface of side planes (Figure 8d), which makes the electric potential around the nanocrystal more

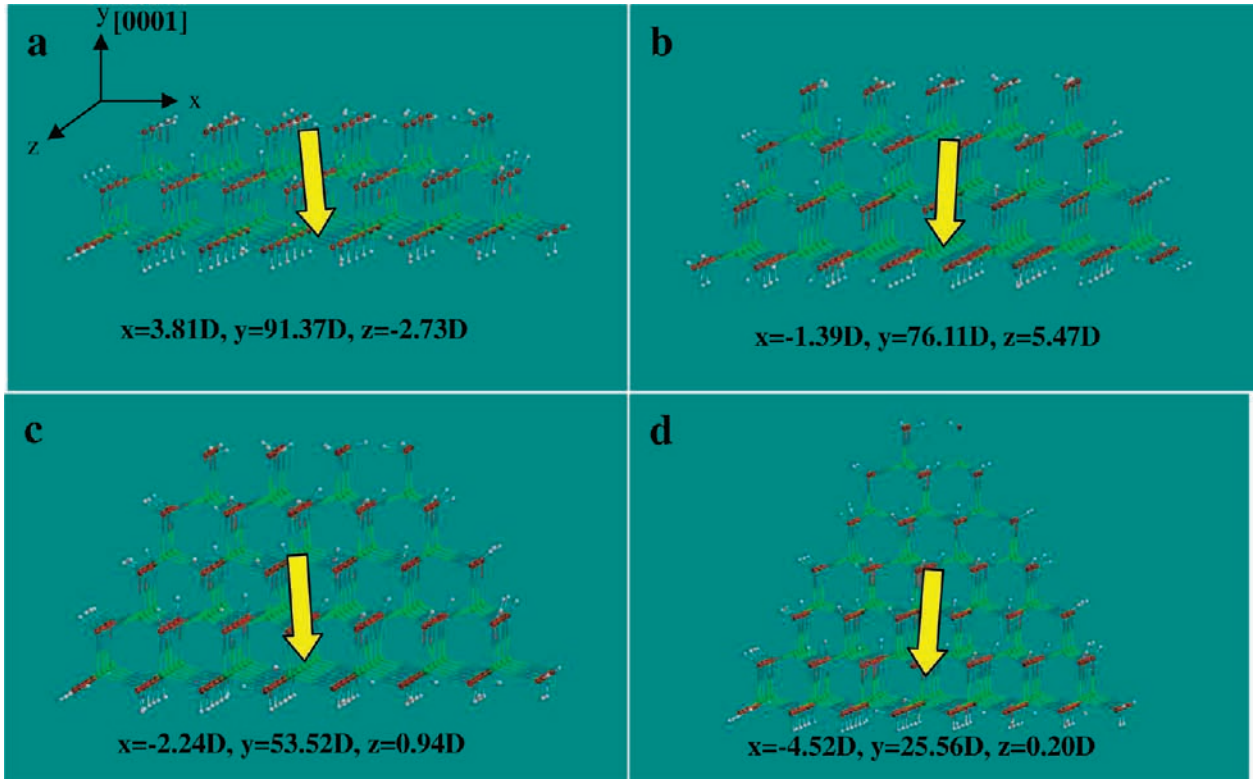

Figure 6. Atomic models in ball and wire mode and corresponding calculation results of dipole moments, *D*, for pyramids with different degrees of truncation. (a) $Zn_{64}O_{19}(OH)_{93}^{3-}$, (b) $Zn_{83}O_{31}(OH)_{100}^{4+}$, (c) $Zn_{95}O_{38}(OH)_{105}^{9+}$, and (d) $Zn_{105}O_{42}(OH)_{111}^{15+}$. The *x*,*y*,*z* values represent the contribution of *D* in the corresponding direction. The yellow arrows highlight the direction of *D* following the standard description of dipole direction from negative to positive. Zn atoms are green, O atoms are red, and H atoms are gray.

Table 2. Summary of Net Formal Charge and *D* for Atomic Pyramidal Model with Different Degrees of Truncation

molecule stoichiometry	net formal charge	dipole moment (*D*)
$Zn_{64}O_{19}(OH)_{93}$	−3	91.49
$Zn_{83}O_{31}(OH)_{100}$	+4	76.32
$Zn_{95}O_{38}(OH)_{105}$	+9	53.58
$Zn_{105}O_{42}(OH)_{111}$	+15	25.96

homogeneous. All of the above contributes to the decrease of the dipole moment as the pyramids grow.

Now let us relate the quantum mechanical calculation results to the experimental observations of the nanocrystal disassembly system. One can discern that the prepared ZnO pyramids show the strong tendency to self-assemble as mentioned before. The tendency toward linear organization of NPs (Figure 2c,d) indicates the strong anisotropic attraction along the central axis of the pyramid, which coincides very well with the quantum mechanical calculations and the existence of the strong dipole moment in ZnO pyramids (Figure 6). Unlike CdTe,[1h] CdSe,[14a] and PbSe,[14b,d] chain-like structures from pyramids can be detected along the individual NPs even without any special treatment. The final "product" existing in solution can be characterized as a state of quasi-equilibrium between the truncated pyramids and the nearly perfect ones. In other words, the high-energy apex atoms in the tip of the pyramid can be easily lost and acquired. So, pyramids with truncation(s) are always present in the solution. They can effectively attach to each other in the dipolar head-to-tail fashion, which we see in several TEM images here (Figures 1a,b, 2c,d, 3i,j). This results in the assembly of truncated ZnO pyramids (Figure 2d), which can be related to the oriented attachment processes described before.[1h,7,14] However, when pyramids grow bigger, *D* decreases (Figure 6 and Table 2). The reduction of the attractive force field (*D* in particularly) will favor the disassembly of ZnO pyramids along with their growth. Consequently, the dipolar head-to-tail fashion will be not as stable as in the beginning due to the smaller *D*. From another standpoint, the repulsion force, for instance, Coulombic electrostatic repulsion, between growing pyramids will increase due to more defined crystal planes with positive charges present. Finally, when repulsion forces dominate, the disassembly of chains occurs. The slow growth speed along [0001] direction of pyramids related to the excess zinc acetate present in the media gives the possibility for us to observe the disassembly phenomena of chains in the final stage.

To reassemble the NPs, one needs to have a tool to shift the balance between repulsion and attraction. Considering the fact that ZnO pyramids spontaneously disassemble (Figure 3), the repulsion forces generally dominate between these particles. So, we need to increase the attractive component of the interparticle energy. In this respect, one can also say that the entire art of self-organization of NPs is to dial in the strength of the attractive component in a very balanced manner. We first tried to neutralize positive charge of our particles by adding sodium dodecyl sulfate (SDS) or poly(acrylic acid) (PAA). Precipitation indeed occurs, but the agglomerates forming with these coagulants do not exhibit any trace of organization. This indicates that attraction is too strong now, disbalanced, and/or the anisotropy of interactions between NPs is reduced by the presence of the fairly thick and "hairy" SDS or PAA layer. The rigidity of PAA is apparently not high enough to prevent the collapse of a potentially linear NP chain templated by the polymer into a disorganized structure.

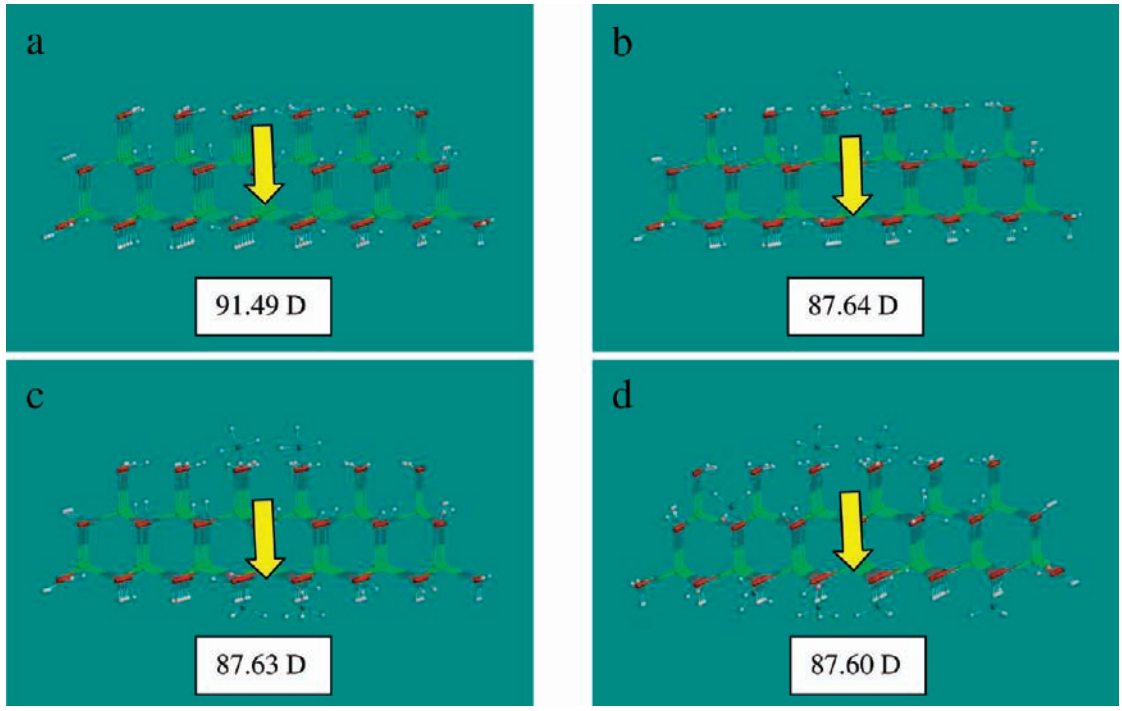

Figure 7. Atomic models in ball and wire mode and corresponding calculation results of *D* with different number of surface methanol molecules. (a) $Zn_{64}O_{19}(OH)_{93}^{3-}$ (0 methanol), (b) $Zn_{64}O_{112}H_{92}CH_3^{3-}$ (1 methanol), (c) $Zn_{64}O_{112}H_{89}(CH_3)_4^{3-}$ (4 methanol), and (d) $Zn_{64}O_{112}H_{85}(CH_3)_8^{3-}$ (8 methanol). The yellow arrows highlight the direction of *D* following the standard description of dipole direction from negative to positive. The corresponding number in each image shows the magnitude of *D*. Zn atoms are green, O atoms are red, H atoms are white, and C atoms are gray.

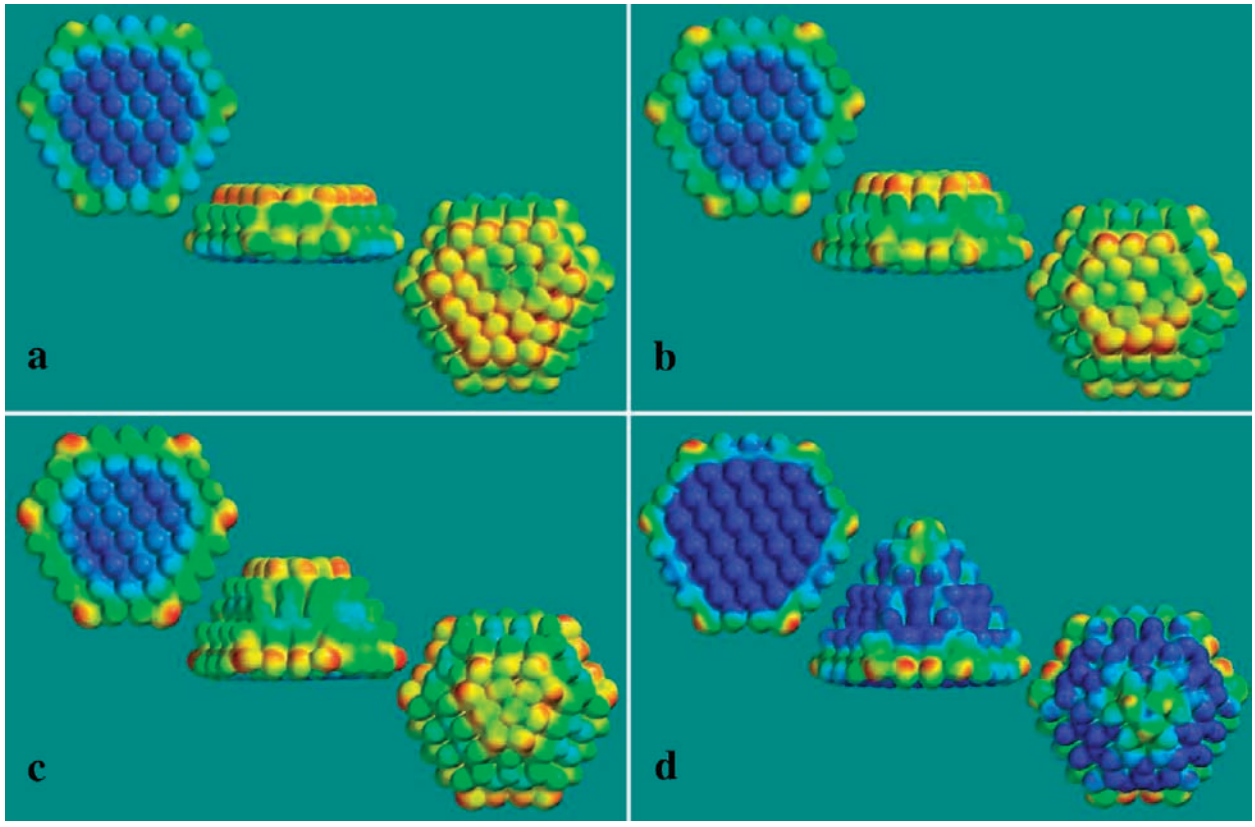

Figure 8. Electrostatic potential mapping for atomic pyramidal models with different degrees of truncation from different angles of view. (a) $Zn_{64}O_{19}(OH)_{93}^{3-}$, (b) $Zn_{83}O_{31}(OH)_{100}^{4+}$, (c) $Zn_{95}O_{38}(OH)_{105}^{9+}$, and (d) $Zn_{105}O_{42}(OH)_{111}^{15+}$. The colors indicate values of the electrostatic potential evaluated on the surface; colors toward the red correspond to negative electrostatic potential, while colors toward the blue correspond to positive electrostatic potential (the colors are set by software designer). In Spartan software used in this Article, the direction of dipole moment is set to point from positive (blue) to negative (red), which is opposite of conventional notations for dipole directions.

We succeed in controlling the aggregation process, reaching the fine balance between attraction and repulsion, and reassembling pyramids into chains by using a similarly charged polymer, that is, cationic poly(dimethyldiallylammonium bromide), PDDA. Notably, all of the previous studies of polymer-induced NP assembly in chains were based on the use of electrostatic interaction with oppositely charged polymers.[1e,24]

Because of the strong positive charge present on both ZnO NPs and the polymer, PDDA does not form polymer−NP aggregates with ZnO pyramids but rather forces the NPs together via excluded volume interactions. These kinds of interactions between nonabsorbing similarly charged polymers and micrometer-scale colloids (especially hard spheres) have been extensively studied for large microscale colloids.[25,26] This is not the case for the nanometer scale particles, however. Surprisingly, there are no studies of the effect of excluded volume interactions on NP superstructures except the recent experiment+simulation study in which these interactions were automatically included as a part of the code for Monte Carlo calculations.[4a]

The nature of excluded volume interactions is quite different than those forces we discussed before and is worth a brief introduction. The pioneering theoretical work from Asakura, Oosawa, and Vrij[26] pointed out that when the distance between two colloidal particles becomes smaller than the diameter of the added polymer coils, the polymer is excluded from that region (depletion zone), and the resulting imbalance in the osmotic pressure gives rise to an effective attraction between the colloids. The addition of nonadsorbing polymer to a stable colloid may destabilize the dispersion when a certain threshold of polymer concentrations is exceeded. This effect creates a powerful force that can be "dialed" experimentally very easily. Also important, the excluded volume interaction can be greatly intensified when the macromolecules are charged, and, in such a case, a macroscopic aggregation of suspended particles can take place.[26a] Calculations also show that the interplay of more subtle forces, such as polymer−polymer interactions,[27] and the effects of charge on the colloids and polymers[28] can lead to more complex agglomeration behavior.[29] Note that the relative size of polymer chains and particles also has great significance for excluded volume interactions. For all of these reasons, nanocolloids are likely to demonstrate new more sophisticated agglomeration patterns than microcolloids. The effect of nanoscale dimensions can be further enhanced by substantially stronger anisotropy of NPs.

Let us now come back to the system at hand comprised of PDDA and ZnO pyramids. In complete agreement with the general description of excluded volume interactions above, PDDA forces ZnO pyramids to self-assemble with each other. Osmotic pressure provides additional attractive force counterbalancing the electrostatic repulsion. Moreover, using the established shapes of NPs (Figures 2 and 3), we can deduce interesting organizational details of the produced ZnO assemblies. Considering the previous studies with CdTe,[1e,h,i,4,24] this can be a real advantage because the geometry of ZnO pyramids is more distinct and this material is more stable under electronic beam.

Table 3. Dynamic Light Scattering Measurement of the Average Size of Nanocolloids with Different Aging Time after the Addition of PDDA

aging time after the addition of PDDA (h)	0.5	3	5	8
average size (nm)	91.33	173.90	407.80	429.00

First, we can see a gradual growth of the ZnO assemblies both in DLS data and in TEM images after addition of PDDA (Table 3 and Figure 9). The light scattering measurements (Table 3) indicate the increase of the average particle size along with more aging time implying the dynamic nature of the assembly process induced by excluded volume interactions, which can be further confirmed by analysis of TEM images (Figure 9). One interesting feature to point out in the assembly patterns in Figure 9 formed immediately after addition of PDDA is that the pyramids change their preferential mode of attachment to each other from the anticipated head-to-tail sequence (Figures 2 and 3) to tail-to-tail NP pairs (Figure 9a−h). Assuming that the direction of the dipole of NPs is not affected by PDDA, such change in packing corresponds to the drastic change of the self-assembly pattern in Figure 2c from the overall attractive contribution of the dipole−dipole interaction to the repulsive dipole−dipole energy. It can be a nice demonstration of the relative strength of the excluded volume interactions in the overall balance of forces between the NPs. What is also important is that the ZnO particles do not fuse together and retain separate crystal lattice structures separated by a gap between them (Figure 10). Nevertheless, there is an obvious correspondence of atomic layers between adjacent particles originating probably from the short-range atomic interactions (Figure 10). This structural independence allows the crystals to rearrange when needed. It is noted that the surface charge balance can also be achieved by the bilayer formed from surfactants templating the formation of ZnO platelets pairs in a similar pattern.[8e]

Not surprisingly, the tail-to-tail pairs of NPs are apparently metastable, and further aging results in the formation of long chain-like structures (Figure 9i−p). If aging takes place more than 12 h, precipitation is detected. The observed chains are probably the result of the reorganization of the initial pyramidal pairs in Figure 9a−h by flipping one of the pyramids. In Figure 9i,j, one can recognize the antiparallel fashion of dipolar packing, which gives the overall attractive dipole−dipole interparticle energy component. Besides the obvious head-to-tail sequence, such arrangement of tetrahedral pyramids was previously predicted from simulations as a plausible one for the formation of the NP chains[4f] but never confirmed experimentally due to the cited experimental features of CdTe. ZnO pyramids in Figure 9i−p give excellent demonstration that indeed the NP chains can be organized in such way. The entire set of data on the ZnO−PDDA system indicates that the

(24) Srivastava, S.; Kotov, N. A. *Soft Matter* **2009**, *5*, 1146–1156.
(25) (a) Tuinier, R.; Fleer, G. J. *Macromolecules* **2004**, *37*, 8764–8772. (b) Fortini, A.; Bolhuis, P. G.; Dijkstra, M. *J. Chem. Phys.* **2008**, *128*, 024904. (c) Bolhuis, P. G.; Louis, A. A.; Hansen, J. P. *Phys. Rev. Lett.* **2002**, *89*, 128302. (d) Tuinier, R.; Aarts, D.; Wensink, H. H.; Lekkerkerker, H. N. W. *Phys. Chem. Chem. Phys.* **2003**, *5*, 3707–3715. (e) Bleha, T.; Cifra, P. *Langmuir* **2004**, *20*, 764–770.
(26) (a) Asakura, S.; Oosawa, F. *J. Polym. Sci.* **1958**, *33*, 183–192. (b) Asakura, S.; Oosawa, F. *J. Chem. Phys.* **1954**, *22*, 1255–1256. (c) Vrij, A. *Pure Appl. Chem.* **1976**, *48*, 471–483.
(27) (a) Moncho-Jorda, A.; Rotenberg, B.; Louis, A. A. *J. Chem. Phys.* **2003**, *119*, 12667–12672. (b) Schmidt, M.; Denton, A. R.; Brader, J. M. *J. Chem. Phys.* **2003**, *118*, 1541–1549.
(28) (a) Denton, A. R.; Schmidt, M. *J. Chem. Phys.* **2005**, *122*, 244911. (b) Ferreira, P. G.; Dymitrowska, M.; Belloni, L. *J. Chem. Phys.* **2000**, *113*, 9849–9862. (c) Fortini, A.; Dijkstra, M.; Tuinier, R. *J. Phys.: Condens. Matter* **2005**, *17*, 7783–7803.
(29) Striolo, A. *Phys. Rev. E* **2006**, *74*, 041401.

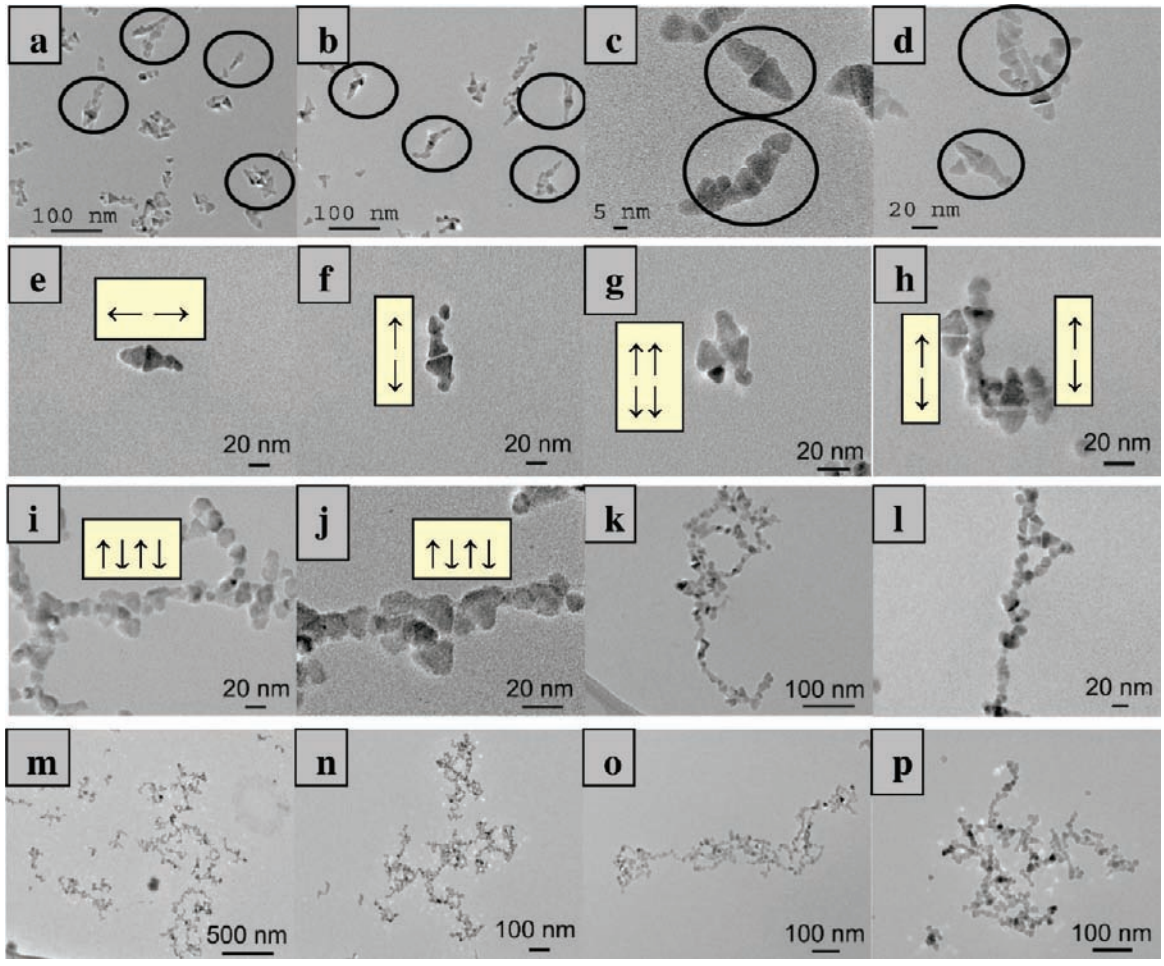

Figure 9. TEM images of ZnO pyramids solution after adding PDDA for (a−h) 30 min, (i−l) 5 h, and (m−p) 12 h.

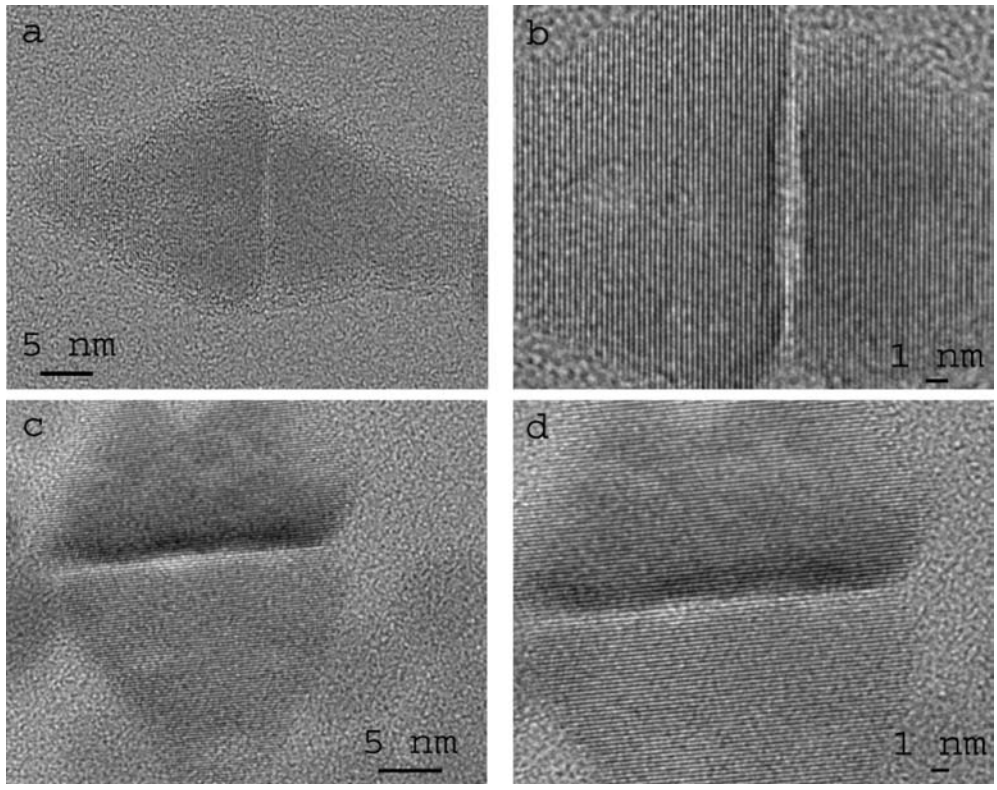

Figure 10. HRTEM images of tail-to-tail pyramid pairs.

organization of dipoles in particle assemblies is quite dynamic and can be controlled by appropriate experimental conditions.

Conclusions

A simple method to synthesize ZnO hexagonal pyramids with strong anisotropy of interparticle interactions has been established. Before they form a dispersion of nearly perfect hexagonal pyramids, the starting ZnO NPs undergo several stages of gradual recrystallization and restructuring from amorphous spheres to clustered plates, agglomerated truncated pyramids, NP chains, and individual pyramids. Repulsion forces dominate the interparticle interactions in such dispersions, because the dipole moments of pyramids are progressively reduced as they become more and more complete. The reassembly of the ZnO pyramids into chains can be achieved via engaging excluded volume interaction after adding a similarly charged polymer. This can be a powerful method for assembling a variety of NPs into complex structures. Geometrical organization of pyramids in the new chains provides clear demonstration of variability of the relative orientation of dipoles including head-to-tail, tail-to-tail pairs, and antiparallel chains. This finding represents important fundamental knowledge and will be used for the design of the optoelectronic materials in the future. Also, we expect that fine-tuning of the conditions of ZnO assembly with PDDA and other polymers can lead to quite sophisticated 3D superstructures spanning the nano- and microdimensions. Improving uniformity of ZnO pyramids should help in building a more regular NP system in the subsequent studies but should not be achieved for the expense of great reduction of anisotropy.

Acknowledgment. We thank the National Science Foundation (NSF), Air Force Office of Scientific Research (AFOSR), and Department of Energy (DOE) for the support of this research with the following grants: AFOSR-GRT00008581/RF60012388; AFOSR-444286-P061716; AFOSR−AFOSR, FA9550-08-1-0382; NSF-ECS-0601345; NSF-R8112-G1; NSF-0932823; NSF-0933384; NSF-0938019.; DOE DE-SC0000957.

JA906868H